Spectrochimica Acta Part A: Molecular and Biomolecular Spectroscopy 337 (2025) 126148

Contents lists available at ScienceDirect

Spectrochimica Acta Part A:
Molecular and Biomolecular Spectroscopy

journal homepage: www.journals.elsevier.com/spectrochimica-acta-part-a-molecular-and-biomolecular-spectroscopy

Examining the adsorption and sensing characteristics of cytosine (CTE) on Y9N9 (Y = Al, B, Ga) nanorings using solvent effects, DFT, AIM and SERS analyses

Jamelah S. Al-Otaibi [a,*], Y. Sheena Mary [b], Unnati Jethawa [c], Brahmananda Chakraborty [d,e], Maria Cristina Gamberini [f]

[a] Department of Chemistry, College of Science, Princess Nourah Bint Abdulrahman University, P.O. Box 84428, Riyadh 11671, Saudi Arabia
[b] Department of Physics, FMN College (Autonomous), Kollam, Kerala, University of Kerala, India
[c] Department of Physics, SIES College of Arts, Science & Commerce, Mumbai 400022, India
[d] High Pressure &Synchroton Radiation Physics Division, Bhabha Atomic Research Centre, Trombay, Mumbai 400085, India
[e] Homi J Bhabha National Institute, Bhabha Atomic Research Centre, Trombay, Mumbai 400085, India
[f] Department of Life Sciences, University of Modena and Reggio Emilia, via G. Campi 103, 41125 Modena, Italy

HIGHLIGHTS

- Sensing applicability of the cytosine (CTE)-Y9N9 (Y = Al, B, Ga) nanorings.
- CTE recovery time indicates that it can be used to extract or store CTE depending on the environment.
- RDG analysis, gives the nature and strength of the interaction in both vacuum and aqueous medium.

GRAPHICAL ABSTRACT

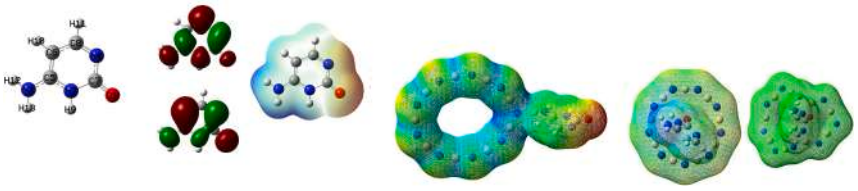

ARTICLE INFO

Keywords:
DFT
Cytosine
Nanorings
Adsorption
Reactivity analysis

ABSTRACT

Nucleobases are nitrogenous biological compounds that are more significant in a range of biological and in medical applications. They are constituents of nucleotides in deoxyribonucleic acid (DNA) and ribonucleic acid (RNA). Therefore, we assessed the sensing applicability by studying the cytosine (CTE)-Y_9N_9 (Y = Al, B, Ga) nanoring interaction using density functional theory. It was evident that CTE interacted strongly with each ring. Due to charge transfer between the nanoring and CTE, a dipole moment (DM) is generated. All complexes have band gaps less than that of CTE. Complexes' band gap energies are lower in aqueous phase and vacuum than they are in pristine rings. All complexes exhibit higher adsorption energies in solvent medium in comparison with that in vacuum. Changes in the frontier molecular orbitals (FMOs) energies of nanorings after interaction have a major impact on their electrical conductivity and work function. In addition to being an electrical sensor, the Y_9N_9 nanorings for CTE can also be utilized as a work function-based sensor. But Y_9N_9's CTE recovery time indicates that it can be used to extract or store CTE depending on the environment. The current work can be expanded to examine the impact of Ag/Au/Cu doping using Y_9N_9 in order to examine the characteristics of drug delivery carriers and the consequence of doping. The interaction between the analyte and substrate was further studied using reduced density gradient (RDG) analysis, comparing the nature and strength of the interaction in both vacuum and aqueous medium. The observations revealed a stronger interaction in the presence of an aqueous medium, which aligns with the higher adsorption energy values.

* Corresponding author.
E-mail addresses: jamelah2019@rediffmail.com, jsalotabi@pnu.edu.sa (J.S. Al-Otaibi).

https://doi.org/10.1016/j.saa.2025.126148
Received 20 May 2024; Received in revised form 24 March 2025; Accepted 30 March 2025
Available online 31 March 2025

1. Introduction

Carbon atoms can combine in a variety of ways to create several allotropes with unique hybridizations. Various carbon allotropes can be found in materials such as diamond, graphite, bucky balls, and others. Due to the differences in structural geometry and hybridization, these allotropes display unique physical and chemical properties [1,2]. Diamond, for instance is a crystal that is incredibly transparent and hard and acts as an insulator. Conversely, graphite is electrically conductive and flaky [3–5]. The most flexible carbon allotrope, graphene, has several amazing properties [1,2]. Furthermore, other allotropes, such as fullerenes and carbon nanotubes, have unique properties of their own [6]. These materials' mechanical, optical and thermal characteristics are well known.

Although several nitrides have been investigated both theoretically and empirically, boron and aluminum nitrides are the most sought-after due to their remarkable characteristics [7,8]. The unadulterated AlN exhibits chemisorption with NH_3, but only slight interactions with dangerous gas molecules [7]. The physisorption behavior of boron and aluminum nitride nanotubes with CO and NO is similar [8]. NH_3 and aluminium/boron nitride nanotubes have a substantial interaction [9,10]. Similarly, $B_{12}N_{12}$ fullerene is a good NH_3 sensor on its own, but it's not the greatest choice for CO and NO detecting [11]. Synthesis of BN-polycyclics and identification of novel azaborine chemistry characteristics are reported [12]. The solvothermal approach of Guo et al.'s pyrene-based metal organic framework (MOF) synthesis was able to detect the presence of water in common organic solvents [13]. There is a literature on a theoretical study of fluorouracil adsorption on B-, Al-, Ga-doped C_{36} nanotubes [14]. Zinc oxide nanoclusters were used to demonstrate the chemisorbed nature of CO_2 and physical adsorbed nature of CH_4 through their adsorption [15].

An analysis using DFT shows that the Al_6N_6 is a useful NH_3 sensor [16]. Science predicts that in addition to group-III element based nitrides are using for detection purposes [17,18]. Earlier studies have shown how crucial it is to create nanomaterials with superior sensing qualities in order to identify dangerous gases [17,18]. Report on the interaction between C_{18} (Y_9N_9: Y = Al, B) and its predicted allotropes is in literature [19]. Hasnain et al., looked into the sensing mechanisms of C_{18} [20]. Additionally, a variety of adamantine derivatives are used in the investigation of medicinal compounds over B_9N_9 and their interactions with varied surroundings [21]. However, Y_9N_9(Y = Al, B, Ga) has to be thoroughly investigated for drug detection. Recently, there has been reporting on the interaction between oxadiazoles and pure and B/Al/Ga-doped C_{60} [22]. Theoretical reports of fluoroquinolone adsorption on the surface of C_{60} doped with magnesium, calcium, iron and zinc are presented [23].

Theoretical reports of ZnO nanoclusters' size-dependent adsorption ability for drug carrier systems are in literature [24]. Recently, an investigation on the pharmacological interaction between favipiravir and BN-doped C_{60} for drug carrier systems was published [25]. Linsmeier et al., have reported on the stability of GaP, and their results corroborate the idea that GaP is poisonous [26]. Gallium nitride is non-toxic and biocompatible both before and after functionalization with peptides [27]. BN nano spheres are potentially biocompatible material that is more biocompatible at lower concentrations than water soluble BN nano material [28].

The therapeutic paradigm has substantially evolved in the last few years thanks to the theranostic nano medicine, a developing field. Early and extremely accurate detection of clinical complaints as well as efficient therapies are possible with nano medicine [29]. Nucleo bases are nitrogenous molecules that are present in the basic structures of nucleotides in DNA and RNA. They are becoming more and more important in a variety of biological domains, especially in medicinal applications [30]. In DNA and RNA molecules, cytosine joins guanine as a base pair. However, it has intrinsic instability, which makes it prone to spontaneous deamination and conversion to uracil [31,32].

The synthesis, solvent role, absorption and emission study of cytosine derives was reported recently [32]. Cytosine is present within DNA, RNA, and nucleotides. In its capacity as cytidine triphosphate, it exhibits co-factor activity with enzymes, facilitating the transfer of a phosphate group [32]. Cytosine forms a base pair with guanine in both DNA and RNA molecules. There has been recent reportage on the theoretical interaction of Au_{13} nanocluster with nucleic acid bases [33]. The density functional theory (DFT) investigations on cytosine analogs for guanine-induced double-proton transfer were published by Xue et al., [34]. Kim et al., published a theoretical report on the adsorption of cytosine on Si (100) [35]. Using DFT simulations, the adsorptions of nucleo bases over $B_{12}N_{12}$ and $Al_{12}N_{12}$ were also investigated [36]. Furthermore, compared to its $Al_{12}N_{12}$, the $B_{12}N_{12}$ nano cluster exhibits weak adsorption and high sensitivity towards nucleo bases [36]. The theoretical study of hydroxyl radical reactivity with cytosine and thymine are studied [37]. In experimental setting, artificial cytosine analogs were complexes to create silver arrays inside DNA duplexes [38]. The DFT study of nucleo bases cytosine on on zinc oxide-graphene and platinum decorated graphene was reported [39,40].

Cytosine has been considered for quantum computation since 1998, when researchers at Oxford University developed nuclear magnetic resonance quantum computer based on cytosine [41]. Adsorption of cytosine on Si and Ge doped graphene are reported theoretically [42]. Fan et al., reported the high performance TadA-8e derived cytosine and dual base editors with undetectable off-target effects in plants [43]. Synthesis, solvent role, absorption and emission studies of cytosine

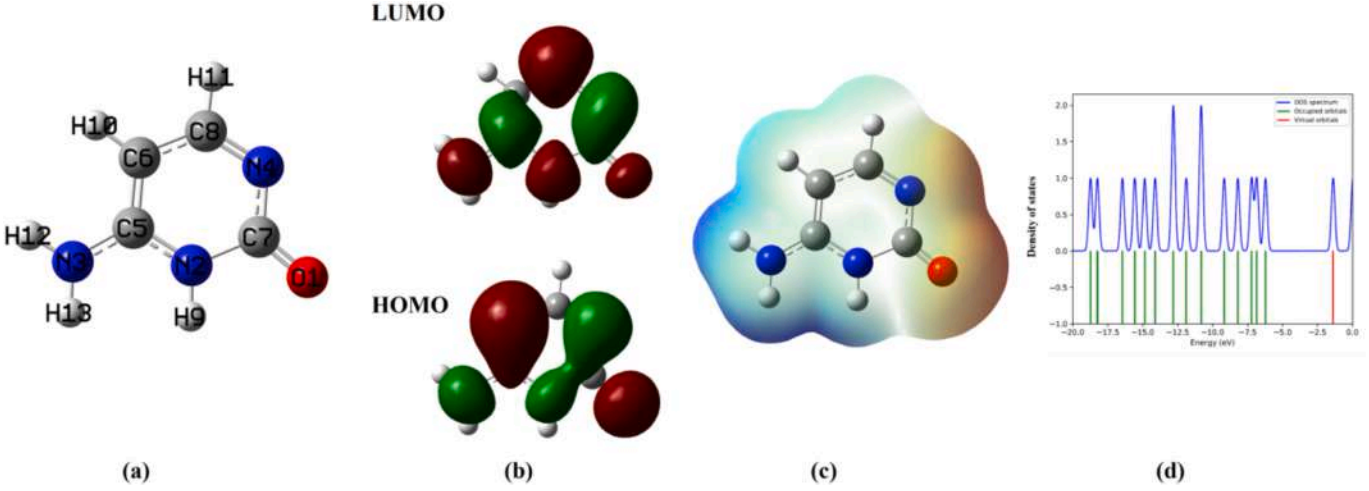

Fig. 1. CTE's (a) optimized geometry (b) FMOs (c) MEP (d) DOS spectrum.

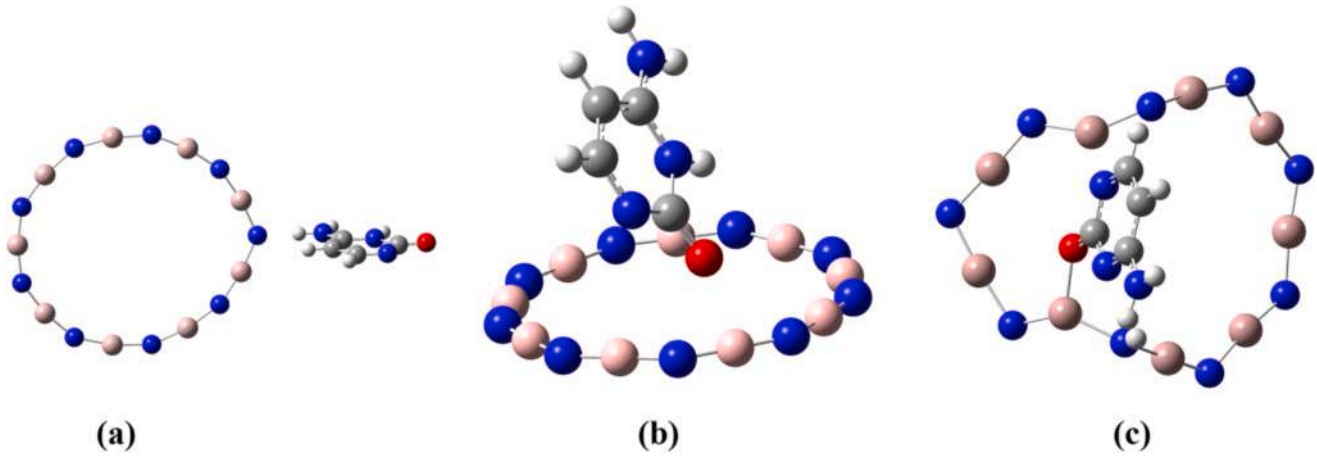

Fig. 2. Optimized geometry of CTE with (a) Al_9N_9 (b) B_9N_9 (c) Ga_9N_9.

derivative were reported recently [32]. Parkinson et al., reported the harnessing cytosine for tunable nano particle self assembly behavior using orthogonal stimuli [44]. It is stated that a fluorophore molecule placed in Tb-MOF functions as a chemo sensor to detect bacterial spores [45]. Surface enhanced Raman scattering (SERS) has been widely used in science because it greatly increases the samples' intrinsically weak Raman emissions [46]. Because of the charge transfer caused by chemical interaction between nanosurfaces and adsorbates, the Raman intensity is very much boosted [46].

The cytosine, a nucleo bases are nitrogenous molecules that are present in the basic structures of nucleotides in DNA and RNA, a key pharmacore of several non-nucleoside chemotherapeutic agents and its derivatives have been developed as anticancer, antiviral agents etc., [47]. Hence in order to understand the adsorption nature of cytosine, in this work we have investigated cytosine's adsorption on nano rings. Motivated by the previously mentioned details as well as the literature review, we have investigated the interaction of CTE over Y_9N_9 nano rings by density functional theory (DFT) simulations. The effect of nano rings as an adsorbent for CTE is examined theoretically in the present report.

2. Methods

DFT calculations are performed using the Gaussian16 software using B3LYP/def2-TZVPPD technique for Y_9N_9 nano ring optimization, which works well for parent material study (C_{18}) in vacuum and solvent (**water)** [48]. This basis set is ideal for the computation because it is a diffuse-augmented variations function [49]. We used the same basis set and methods to find the properties of Y_9N_9. FMOs, structural analysis and the charge population from natural bond orbital (NBO) analysis were all displayed using the Gaussview software [50]. Density of states (DOS) spectra was plotted using GaussSum software [51]. Figs. 1 and 2 depict the optimum CTE geometry (with FMOs, molecular electrostatic potential (MEP) and DOS spectra) and CTE-nano rings. The 2D-RDG scatter plots and 3D-RDG isosurfaces were produced utilizing the Multiwfn [52] and VMD [53] software tools. The RDG function s(r) assesses deviations from a uniform electron distribution and is defined by:

$$s(r) = \frac{1}{2(3\pi^2)^{1/3}} \frac{|\nabla\rho(r)|}{\rho(r)^{4/3}}$$

3. Results and discussion

3.1. The Y_9N_9 nano rings

Fig. 3 shows Y_9N_9 nanorings and the bond lengths of B_9N_9, Al_9N_9, and Ga_9-N_9 are 1.32/1.70/1.76Å for B/Al/Ga-N. The angles around N and B are 147° and 173°. For Al_9N_9, angles around N and Al are 152° and 168°. The angles N and Ga of Ga_9-N_9 are 130° and 170°.

Al_9N_9, B_9N_9, and Ga_9-N_9 have energy gap (Eg) of is 3.52, 6.03, and 3.40 eV (Table 1) which agrees with DOS (Fig. S1). The Fermi energy (EF) values for Al_9N_9, B_9N_9, and Ga_9-N_9 are −4.37, −4.58 and −4.81 eV, respectively. The nano rings structural properties, highest occupied

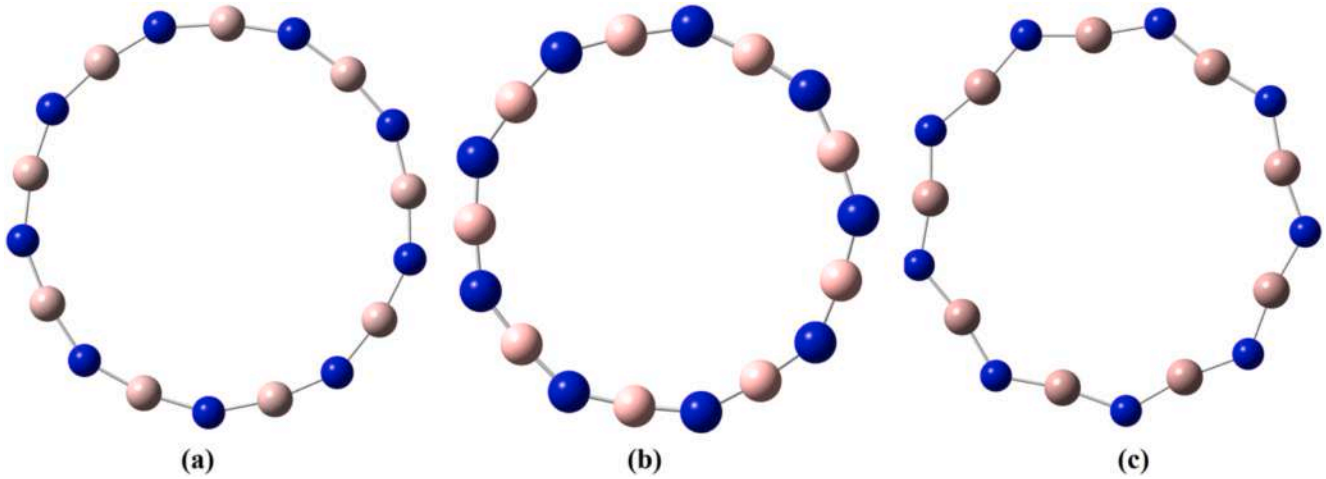

Fig. 3. Optimized geometry of (a) Al_9N_9 (b) B_9N_9 (c) Ga_9N_9.

Table 1
Chemical descriptors and changes.

Systems	EH (eV)	EL (eV)	Eg (eV)	ΔEg (%)	η (eV)	μ (eV)	Δϕ (%)	Ω(eV)
CTE	−6.22	−1.38	4.84	–	2.42	−3.80		2.98
Al_9N_9	−6.13	−2.61	3.52	–	1.76	−4.37		5.42
B_9N_9	−7.60	−1.57	6.03	–	3.01	−4.58		3.48
Ga_9N_9	−6.51	−3.11	3.40	–	1.70	−4.81		6.80
Vacuum								
Al_9N_9-CTE	−5.70	−3.08	2.62	−25.58	1.31	−4.39	0.44	7.35
B_9N_9-CTE	−6.73	−1.89	4.84	−19.71	2.42	−4.31	6.03	3.83
Ga_9N_9-CTE	−5.46	−3.32	2.14	−37.07	1.07	−4.39	8.59	9.03
Water								
Al_9N_9-CTE	−6.10	−2.58	3.52	−0.11	1.76	−4.34	0.84	5.34
B_9N_9-CTE	−6.35	−1.47	4.89	−18.89	2.44	−3.91	14.68	3.13
Ga_9N_9-CTE	−5.72	−2.61	3.11	−8.42	1.56	−4.17	13.33	5.58

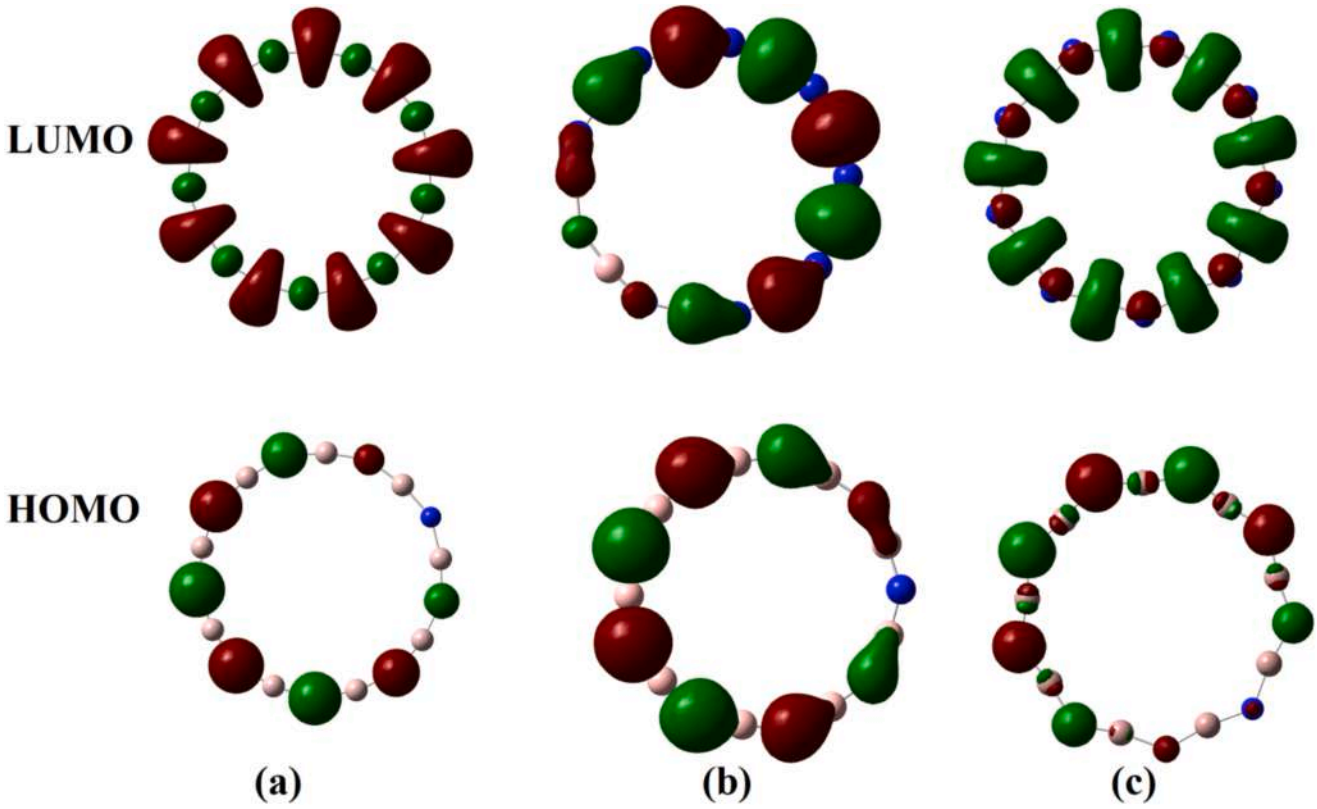

Fig. 4. HOMO-LUMO plots of (a) Al_9N_9 (b) B_9N_9 (c) Ga_9N_9.

molecular orbital energy (EH), lowest unoccupied molecular orbital energy (EL) and energy gap (Eg) are compared and the results are in line with earlier research [19–21,54,55].

For B_9N_9, the energies of the HOMO and LUMO were reported as −9.70 and 0.60 eV respectively, corresponding to an energy gap of 10.30 eV [19]. For Al_9N_9, the HOMO and LUMO energies are −8.73 and −0.93 eV with an energy gap of 7.80 eV [19]. According to Pichierri et al., B_9N_9 nano ring energy gap is significantly larger (9.04 vs 5.71 eV) than that of C_{18} [56]. The reported values of HOMO and LUMO energies of B_6N_6 nano cluster are −9.61 eV and 0.35 eV and for Al_6N_6 nano cluster are −8.81 eV and −1.49 eV, respectively [16]. According to reported literature, the energy gap between HOMO and LUMO for five nucleo bases, adenine, thymine, guanine, cytosine and uracil are 3.81, 3.54, 3.40, 3.68 and 3.92 eV respectively [57].

The HOMO and LUMO energy values for Mg_9O_9 nano ring are −8.62 and −0.18 eV with an energy gap of 8.44 eV [58]. Upon adsorption of a CO molecule onto nano ring, the HOMO and LUMO energy values become −8.52 and −0.13 eV with energy gap 8.39 eV [58]. The calculated value of energy gap of B_9N_9 and Al_9N_9 nano rings is 10.06 and 7.58 eV, respectively according to recent literature [59]. The nano ring has a limited HOMO only over N of B-N bond but for other nano rings, the LUMO is found around B of B_9N_9 and ring (Fig. 4). In CTE-Al_9N_9, HOMO is in CTE and LUMO in Al_9N_9 ring (Fig. 5a). In B_9N_9-CTE both the HOMO and LUMO over CTE (Fig. 5b). For Ga_9N_9-CTE systems, HOMO is over CTE while LUMO is over the nano ring (Fig. 5c). Figs. S2 and S3 displays the IR and Raman spectra of the nanorings; the lack of an imaginary frequency denotes the stability of the nano rings [16].

3.2. *CTE-Y_9N_9 interactions*

For CTE the obtained bond lengths are: C7=O1 = 1.25, C7-N4 = 1.39, C7-N2 = 1.45, C5-N3 = 1.37 and C8-N4 = 1.34 Á. CTE is placed parallel to the nano rings at a separation of 2.5Á in order to maximize the contact between CTE and the latter. The adsorption energy (Table 2),

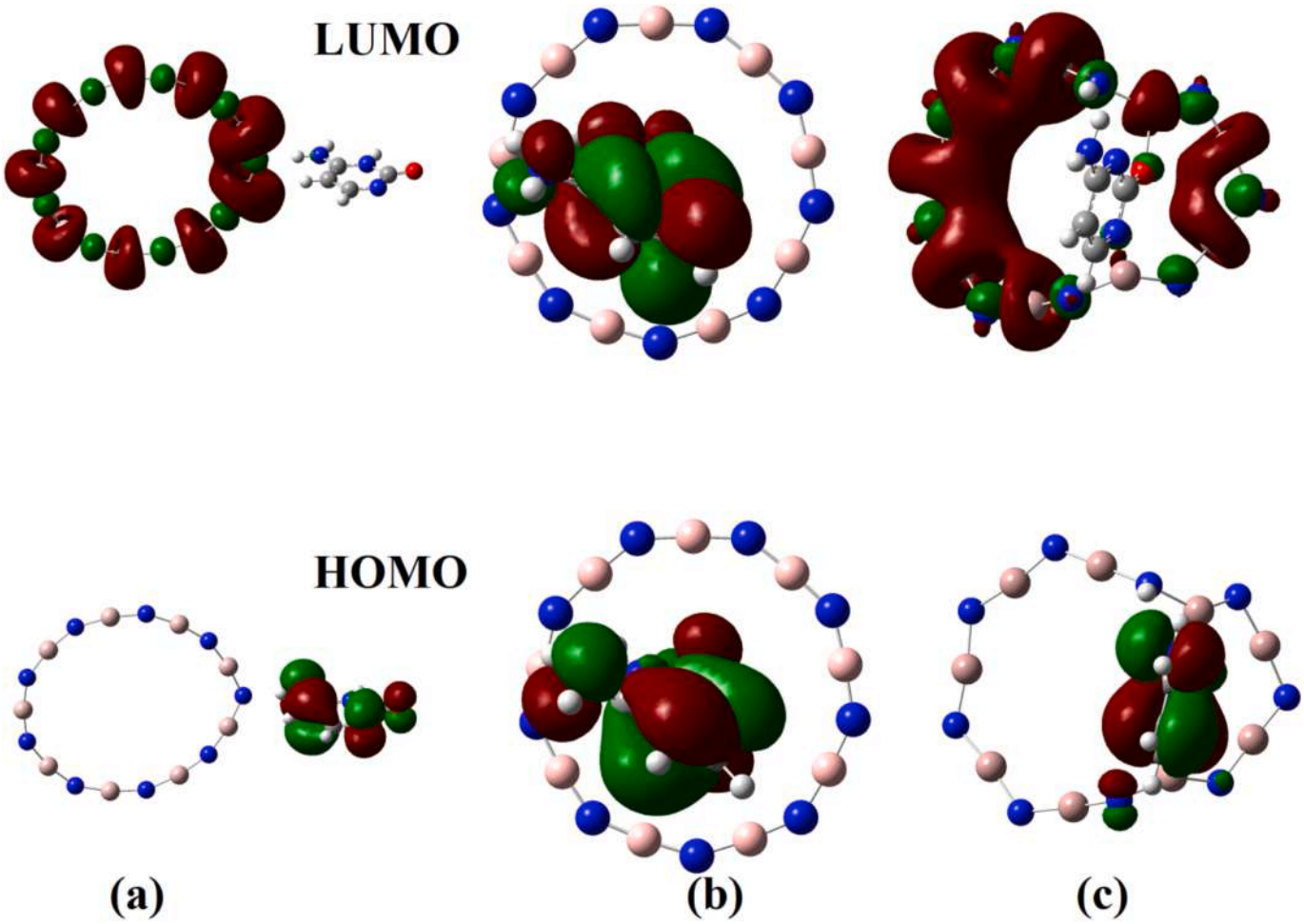

Fig. 5. HOMO-LUMO plots of CTE with (a) Al_9N_9 (b) B_9N_9 (c) Ga_9N_9.

Table 2
Energies, dipole moment, polarizability and adsorption energies.

Systems	Energies (a.u.)	Dipole moment (Debye)	Polarizability (a.u.)	Adsorption energies (kcal/mol)
CTE	−394.857445	9.2451	64.9033	–
Al_9N_9	−2674.824704	0.0040	308.9900	–
B_9N_9	−716.952650	0.0003	184.1860	–
Ga_9N_9	−511.373155	0.0001	347.0693	–
Vacuum				
Al_9N_9-CTE	−3069.698938	12.8671	386.6287	−10.54
B_9N_9-CTE	−1111.823705	9.0894	239.4387	−8.54
Ga_9N_9-CTE	−906.318141	13.6421	391.0483	−54.93
Water				
Al_9N_9-CTE	−3069.770673	15.5849	479.2847	−56.62
B_9N_9-CTE	−1111.851737	13.3666	329.4490	−26.13
Ga_9N_9-CTE	−906.411403	23.9644	522.3123	−113.46

Eads = $E_{(nanoring+CTE)}$ − $E_{(nanoring)}$ − E_{CTE} [60]. The E_{ads} for CTE adsorbed Al_9N_9, B_9N_9, and Ga_9-N_9 are −10.54, −8.54 and −54.93 kcal/mol (vacuum) and −56.62, −26.13 and −113.46 kcal/mol (solvent).

After adsorption, the distances from CTE and Al_9N_9 were found to be 1.80 Å from H12 of NH_2 and 2.84 from N3 to the ring. Here, NH_2 is interacted with the ring and in a nearly perpendicular manner outside the ring. The bond lengths of CTE after adsorption show no significant changes (Table S1). The Al-N length is 1.73Å and angles around N and Al are 132 and 171° near adsorption site. Al-N of CTE-Al_9N_9 increase in comparison to value, 1.70 Å and angles around N and Al for Al_9N_9 are 152° and 168° which becomes 1.73, 132 and 171 after adsorption.

After adsorption, distances from CTE to B_9N_9 were found to be 3.17 and 3.38 from O to B and N. Here, C=O is in a nearly perpendicular order at the centre of the ring. C=O length after adsorption is 1.26Å, C-N lengths of CTE changes as: 1.39 (C7-N4), 1.44 (C7-N2), 1.45 (C5-N2), 1.37 (C5-N3) and 1.34Å (C8-N4) without any significant change (Table S1). B-N lengths are 1.33 Å and 1.32Å near CTE and angles around N and B are 142 and 176° near CTE site. The B-N length in B_9N_9 is 1.32Å and angles around N and B are 147 and 173°, different in CTE-B_9N_9.

Following adsorption, separation between CTE and Ga_9N_9 are 1.95 Å from the bonded O atom to Ga, 2062 from H9 to N of ring and H9 is detached from N2 of CTE, 3.23 from N2 to Ga and 2.15 from N4 to Ga. Here, CTE is nearly perpendicular to Ga_9N_9 within the cavity of the ring. Mainly, the interaction with the ring is through O1 which is bonded to Ga, H9 detached from the NH group and attached with the N atom of ring. Also N4 is near to the ring showing strong interaction in the adsorption. The C=O length is increasing from 1.25 to 1.33Å (Table S1). The C-N lengths of CTE after adsorption are: 1.37 (C7-N4), 1.36 (C7-N2), 1.36 (C5-N2), 1.37 (C5-N3) and 1.37Å (C8-N4) and the variations show strong interaction between CTE with the ring (Table S1). The Ga-N length becomes 1.80 to 1.89 near CTE and angles, Ga-N-Ga/N-Ga-N are 109/137°. The Ga-N distance in Ga_9N_9 is 1.76 Å and angles around N and Ga are 130 and 170°, which are different in CTE-Ga_9N_9.

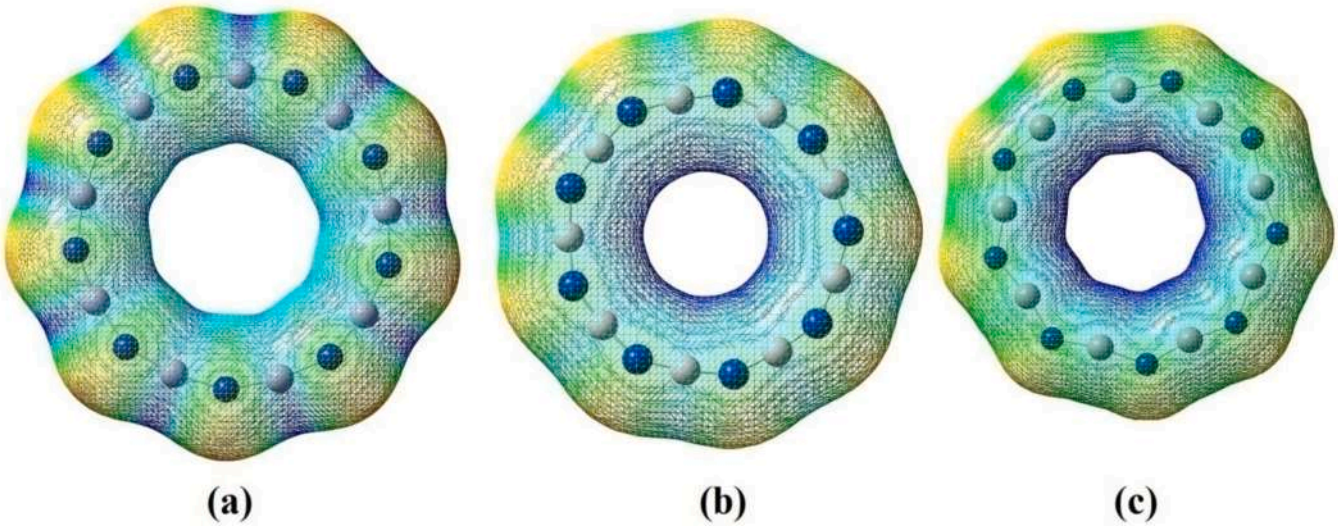

Fig. 6. MEP plots of (a) Al_9N_9 (b) B_9N_9 (c) Ga_9N_9.

Enthalpy values that are negative suggest that adsorption of CTE is exothermic (Table S2). It is evident that CTE adsorption happens spontaneously because all compounds exhibiting CTE adsorption undergo an entropy decrease and computed Gibb's energy changes (ΔG) are negative. Consequently, it is expected that CTE will cling to the nanoring surface spontaneously. For CTE, entropy variations in the Al/B/Ga-N are more negative, at −30.368/-30.868/-58.083 and −24.943/-35.116/-67.069 kcal/mol in vacuum and aqueous phase. There is a greater negative change in the Gibbs energy when CTE adsorption takes place with the Ga_9N_9 nanoring in both phases. The outcome validates that CTE can be applied to nano rings with success [61].

When compared to the polarizability value of CTE and Y_9N_9 rings, all complexes have high values (Table 2). The systems' nonlinear optical features result from an increase in polarizability values in the solvent [62].

3.3. Electronic properties of CTE-Y_9N_9

In general, the NBO charge analysis confirms the interaction [63]. Following adsorption, O1 charge becomes −0.65/-0.67/-0.85e in Al/B/Ga-N ring while that of CTE is −0.64e. For Ga_9N_9-CTE, charge becomes more negative giving strong interaction (Table S3). For N4 and C6 atoms also show variations in value, especially −0.71 for N4 and −0.36 for C6 in GaN adsorption while the pristine values are −0.58 and −0.41e.

Also the interaction with CTE can be connected to change in nanorings' dipole moments [64]. The dipole moment of nano rings is 0.00 because the charge is dispersed symmetrically among their atoms (Table 2). The DM for Al/B/Ga-N becomes 12.8671/9.0894/13.6421 (vacuum) and 15.5849/13.3666/23.9644 Debye (aqueous phase) after contact with CTE; nevertheless, DM for Ga_9N_9 it is high and DM for CTE is 9.2451 Debye. The higher generated DM of CTE adsorbed Ga_9N_9 in this case confirms the strong interaction between the two.

Table 1 shows the calculated work function (ϕ), HOMO and LUMO energy (EH and EL), energy gap (Eg), and changes in Eg of the CTE adsorbed Y_9N_9 [65]. The DOS spectra support these parameters (Fig. S4**).** The Eg of CTE-Y_9N_9 reduced after adsorption in comparison with that of nano rings. The nano ring has a limited HOMO only over N of B-N bond but for other nano rings, the LUMO is found around B of B_9N_9 and ring (Fig. 4). In CTE-Al_9N_9, HOMO is in CTE and LUMO in Al_9N_9 ring (Fig. 5a). In B_9N_9-CTE both the HOMO and LUMO over CTE (Fig. 5b). For Ga_9N_9-CTE systems, HOMO is over CTE while LUMO is over the nano ring (Fig. 5c).

3.4. MEP

MEP is a helpful tool for the interactions between molecular systems. Together with identifying regions of positive (blue), negative (red) and neutral (green) potential, it also find size and shape of the molecule [66]. In the MEP maps, several colors have been employed to represent the various potential intensities. The negative and positive zones are

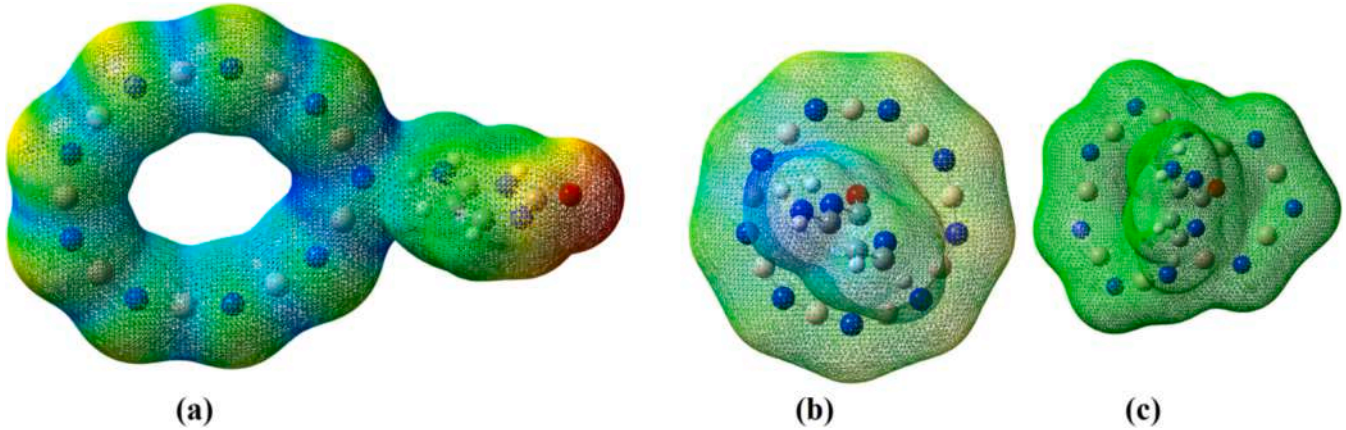

Fig. 7. MEP plots of CTE with (a) Al_9N_9 (b) B_9N_9 (c) Ga_9N_9.

shown in red and blue. The MEP map of every molecule under consideration displays an asymmetric form that results from the presence of metals. The molecules under consideration have a net charge of zero. As a result, the negative charge spreads to the other nanocage sections. Nucleophilic interactions can be therefore occurs in the vicinity of the metal location [67]. Al/B/Ga-N MEP (Fig. 6) shows green and yellow zones in the outer side with blue region in the cavity. The immaculate nano rings have a consistent distribution of green surface. Green zones give neutral potential areas and 0 % electrophilicity, which are non-reactive zones. When CTE is adsorbed, there are changes in potential between atoms, indicating chemisorption of CTE with nano ring (Fig. 7). Additionally, CTE adsorption produces positive potential on CTE and negative potential on Y_9N_9, confirming the NBO charge analysis and the chemisorptions. The uneven pattern of atom charges caused by CTE adsorption creates a variety of reactive regions.

3.5. Sensing properties

The electrical conductivity (σ) gives the sensing relation to CTE and $\sigma = AT^{3/2}\exp(-Eg/2kT)$ [68]. We can deduce that σ is the inverse of Eg at a certain temperature based on the equation presented above. When Eg decreases, there seems to be a significant increase in electrical signal needed to identify CTE. The ΔEg for CTE adsorption over Al/B/Ga-N nano rings are −25.58/-10.71/-37.07 % in vacuum and −0.11/−18.89/−8.42 in aqueous phase (Table 1). These dips in Eg suggest during CTE adsorption, which increases the likelihood that they might be used as sensors.

Any sensor's recovery time (τ), or the expected time needed to desorb every molecule from the complex [65]. For repeated usage, shorte τ are highly desired and $\tau = \upsilon^{-1}\exp(-Eads/kT)$. Here, we have T set to 300 K and υ as 3×10^{12}, 4×10^{11}, 5×10^{10} Hz [69]. B_9N_9 and Al_9N_9 have low τ values for CTE, whereas Ga_9N_9 has a high value in solvent and vacuum (Table S4). The value of τ for CTE over Y_9N_9 is modest in vacuum, and this means that CTE can be stored or eliminated from an environment [69].

For ϕ-type sensors, consideration of the effects of CTE adsorption and ϕ of nanorings is essential. The current density of electrons, $j = AT^2\exp(-\phi/kT)$ [70]. Our findings indicate that the Δϕ for CTE on Al/B/Ga-N is −0.44/6.03/8.59 % (vacuum) and 0.84/14.68/13.33 % (solvent), indicating that they can act as ϕ-type sensor (Table 1).

3.6. Global indices parameter

The estimated global parameters and its change in percentage are displayed in Table 1. Unadulterated Al/B/Ga-N has a μ of −4.37/-4.58/-4.81 eV. The EH and EL values of nano rings changes during CTE adsorption, resulting in a considerable change in μ. The change in μ when CTE interacts with Al/B/Ga-N is 0.44/6.03/8.59 % (vacuum) and 0.84/14.68/13.33 % in aqueous phase. Hardness (η) is a metric for measuring chemical stability of any system; for Al/B/Ga-N, the η values are 1.76/3.01/1.70 eV. In the vacuum and aqueous phase interaction with CTE, all complexes have a decrease in their η values. The electrophilicity index (ω) of Al/B/Ga-N has values 7.35/3.83/9.03 eV (vacuum) and 5.34/3.13/5.58 eV (aqueous phase). When B_9N_9 comes into touch with CTE, the values of ω drop to their lowest levels.

3.7. Raman spectra analysis

In CTE the main bands are at 3633, 3503 cm^{-1} (υNH2), 3464 (υNH), 3135 and 3074 cm^{-1} (υCH), 1642 (υC=O), 1619 and 1585 (δNH), 1538, 1424, 1324, 1014, 980 cm^{-1} (υring), 1282 (υCN of NH2), 1370, 1102 cm^{-1} (δCH), 754 (γCH) (Fig. S5 of CTE). The complexes's IR and Raman spectra are provided in Figs. S6 and S7.

In Al_9N_9-CTE, NH2 and NH stretching modes appear at 3533 and 3457 for Al_9N_9-CTE and the drops in values from that of CTE show the strong interaction with Al_9N_9 nanoring. Also a very strong NH_2 stretching is observed in the complex at 2951 with a very large redshift from that of CTE due to SERS effect. The CH of CTE at 3074 is downshifted to 3054 in Al9N9-CTE due to the adsorption process. CTE's υC=O at 1623 in the complex is lowered by 19 cm^{-1} from that of CTE. The ring modes of complex appear at 1535 and 980 in the complex without any significant shifts. The CH modes of the complex at 1332 and 762 show deviations from that of CTE after adsorption. Bands are at 27, 211, 251, 270, 330, 499 and 1250 cm^{-1} in the Al_9N_9 Raman spectra and in Al_9N_9-CTE these are at 10, 209, 321, 489, 1263 cm^{-1}.

In B_9N_9-CTE, the NH_2 and NH stretching modes appear at 3625, 3487 and 3426 and the decrease in wave number from that of CTE shows the strong interaction with B9N9 nano ring. The υCH of CTE shows no shift in the B_9N_9-CTE. The NH_2 deformation mode of B9N9-CTE complex is present at 1631 while that of CTE 1619 and υCN (NH_2) of complex is at 1290 blue shifted by 8 cm^{-1} from the pristine value. The υC=O of CTE (1642) is 1604 in the complex which is downshifted by 38 cm^{-1}. The ring modes of complex appear at 1535, 1424, and 976 in the complex without any significant shifts. The CH deformation modes of the complex is at 1321, 1115 and 762 with deviation from that of CTE after adsorption. The bands at 2014, 1929 and 521 correspond to B_9N_9 modes. B_9N_9's spectra give bands at 44, 388, 533, 554, 598 and 2044 (Fig. S3) and after adsorption, bands are at 51, 373, 531, 562, and 2004 cm^{-1}.

In Ga_9N_9-CTE, the NH_2 and NH stretching modes appear at 3629, 3483 and 3387 and the reduction in wave number from that of CTE shows the strong interaction with Ga9N9 nano ring. The υCH of CTE (3135) shows no significant shift in the Ga_9N_9-CTE (3139). The NH_2 deformation mode of Ga_9N_9-CTE complex is present at 1608 while that of CTE is 1619 and υCN (NH_2) of complex is at 1274 blue shifted by 8 cm-1 from the pristine value (1282). The υC=O of CTE (1642) appear at 1344 in the complex as υC-O mode which is due to the attachment of O atom to Ga. The ring modes of complex appear at 1573, 1512, and 1240 in the complex with significant shifts. The CH bending modes of complex were at 1110 and 777 with deviations from that of CTE after adsorption. The bands at 920, 552, and 387 correspond to Ga_9N_9 modes. Ga_9N_9's Raman show bands at 17, 102, 151, 341, 407 and 981 cm^{-1} (Fig. S3) and after adsorption, peaks are at 10, 163, 378, 936 cm^{-1}.

The ensuing modified Raman spectra give additional evidence for the tight bond between CTE and the nano rings. SERS enhancement causes the majority of the modes in complexes to be amplified and the complex spectrum contains inactive Raman modes of CTE [71].

3.8. RDG analysis

RDG analysis is an essential tool for gaining insights into both the strength and nature of interactions. It pinpoints the exact atoms and specific sites involved in the interaction, providing a more detailed explanation of the adsorption mechanism.

RDG analysis has been used for developing a gradient corrected functional of increasing quality. By this method, both the nature and strength of the interactions are displaced in the isosurface. The method of RDG is used in this study for assessing the strength and the interaction types of the complex structures through the analysis of the calculated isosurfaces [61] The RDG scatter plot illustrates the relationship between the RDG function s(r) and ρ(r) sign(λ_2), with ρ(r) representing electron density. The Hessian matrix has three eigen values (λ_1, λ_2, and λ_3), and the sign of λ_2 is crucial for determining the nature of the interactions. A positive λ_2 indicates steric interactions, while a negative λ_2 points to covalent or non-covalent interactions. The RDG function s(r) assesses deviations from a uniform electron distribution and is defined by:

$$s(r) = \frac{1}{2(3\pi^2)^{1/3}} \frac{|\nabla\rho(r)|}{\rho(r)^{4/3}}$$

According to this hypothesis, the material's attractive, repulsive and

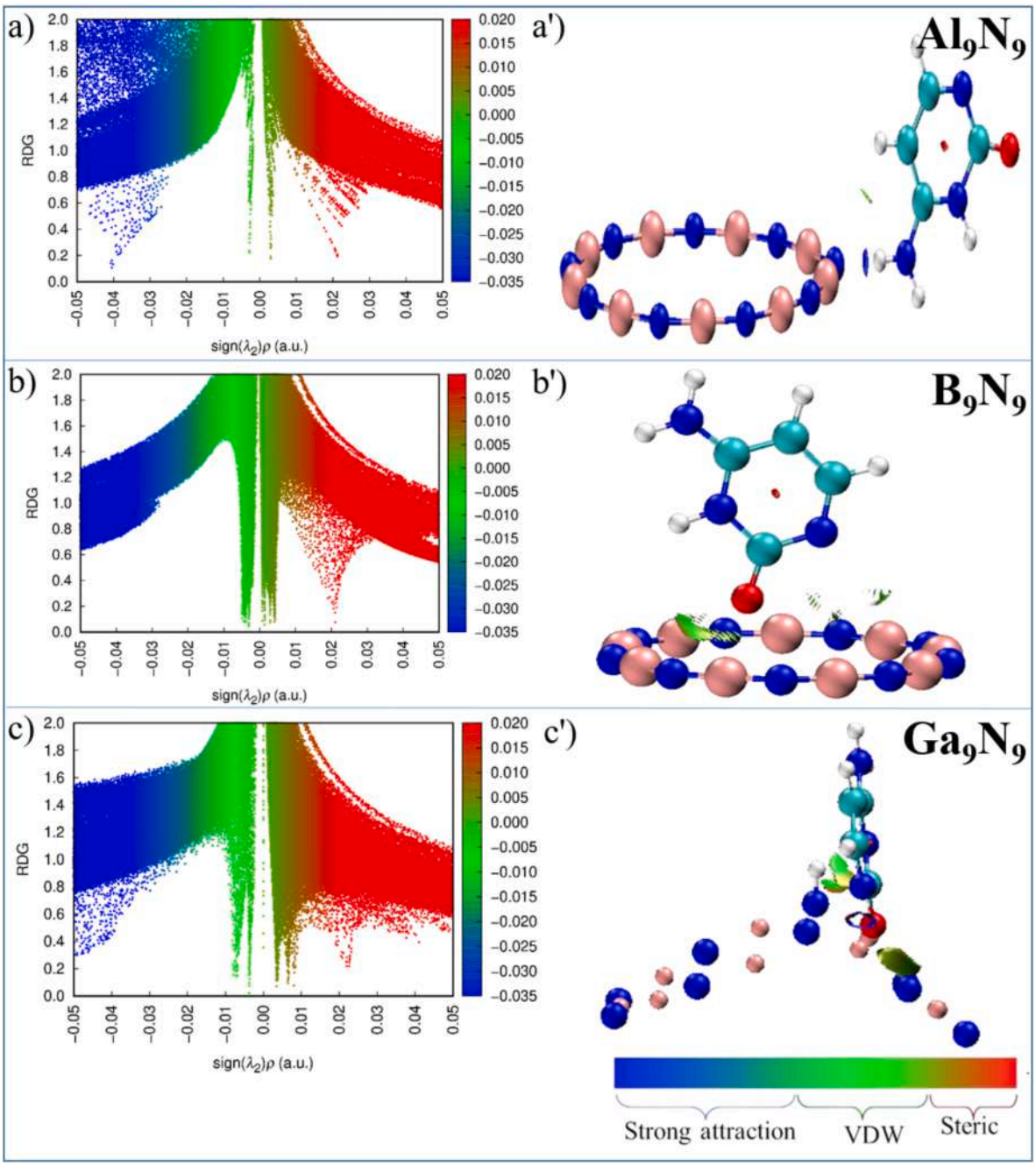

Fig. 8. a–c) 2D RDG scatter plot for CTE adsorbed on Al_9N_9, B_9N_9 and Ga_9N_9 in presence of vacuum, respectively. a'–c') 3D RDG isosurface plot for CTE adsorbed on Al_9N_9, B_9N_9 and Ga_9N_9 in presence of vacuum, respectively.

neutral interactions are represented by the tiny range between negative and positive sign $(\lambda_2)\rho$. In the RDG map, if the sign $(\lambda_2)\rho > 0$, nearly 0 and less than zero are indicating that the repulsive steric effect. Van der Waals interaction and the attractive hydrogen bond interaction, respectively, and their corresponding colours of red, green and blue were also used to identify them [53]. Additionally, red colour give strong steric repulsion, green and greenish-yellow signify van der Waals (vdW) or weak interactions, and blue strong attraction. Fig. 8 (Fig. 9) presents both the 2D RDG scatter plot and the 3D RDG plot, illustrating the interaction of CTE with Al_9N_9, B_9N_9, and Ga_9N_9 nanorings in a vacuum (water).The appearance of green spikes in 2D scatter plot indicates the presence vdW interactions in all cases. The existence of blue disc between H atom of CTE and N atom of Al_9N_9 nanoring indicates strong electrostatic attraction between them. A careful comparison of the 2D scatter plots for CTE interaction with Al_9N_9 in vacuum and in water reveals that the interaction is stronger in the aqueous medium. This conclusion is drawn from the observation that the position of blue spike shifts towards higher electron density in aqueous medium, indicating a stronger interaction compared to that in vacuum [72]. It is also evident that there exists solely vdW interaction between CTE and B_9N_9 nanoring in both vacuum and water. However, these interactions are more pronounced in the aqueous medium. These observations align with the obtained adsorption energy values, which indicate a stronger interaction in the presence of an aqueous medium compared to a vacuum.

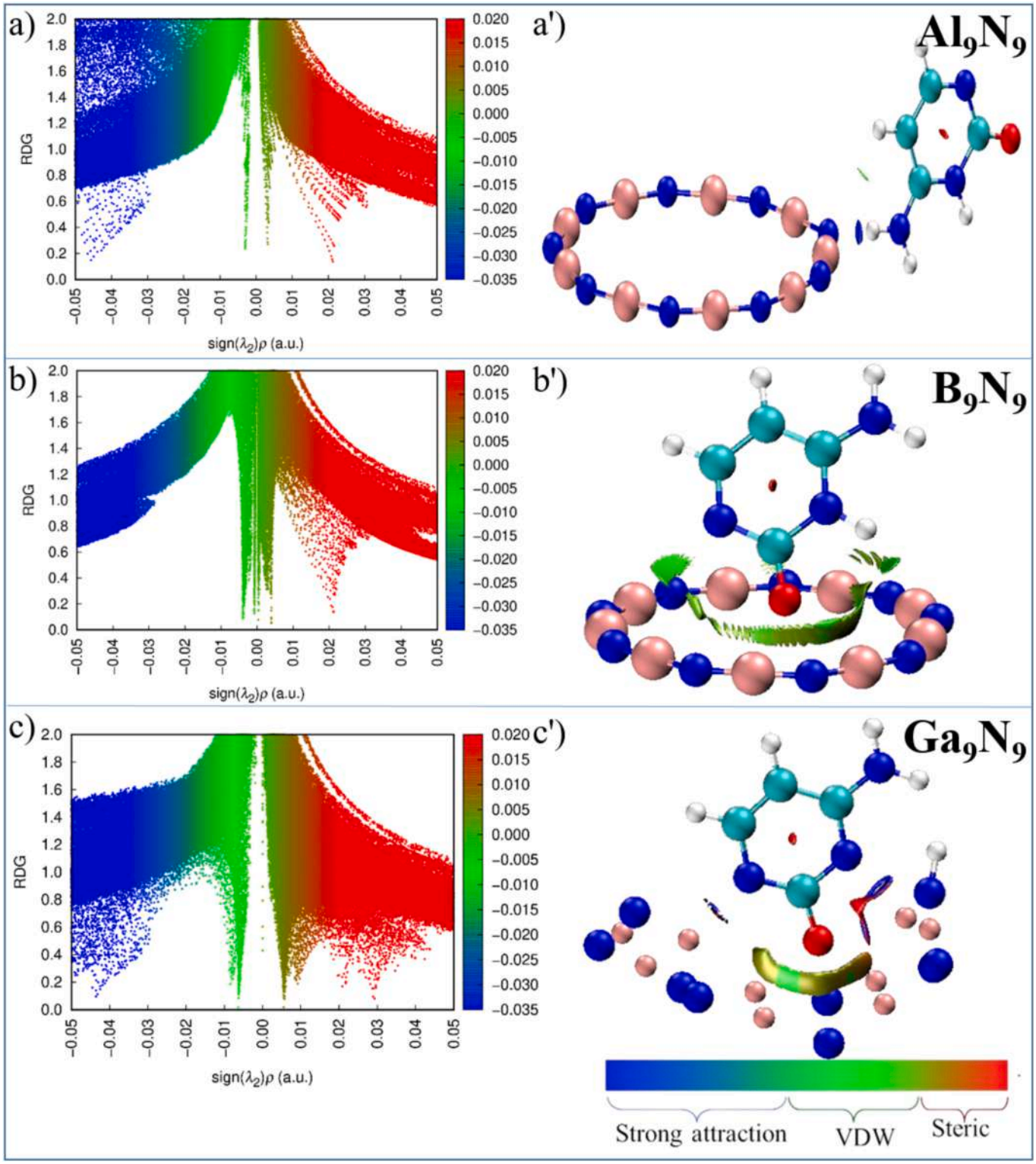

Fig. 9. a–c) 2D RDG scatter plot for CTE adsorbed on Al_9N_9, B_9N_9 and Ga_9N_9 in presence of water, respectively. a'–c') 3D RDG isosurface plot for CTE adsorbed on Al_9N_9, B_9N_9 and Ga_9N_9 in presence of water, respectively.

4. Conclusion

To sum up, we have explored the potential of Y_9N_9(Y = Al, B, Ga) for CTE sensing using DFT analysis. The structural and dynamical stabilities of Y_9N_9 are confirmed by IR spectra. The chemisorption interaction of CTE with nano rings is supported by the adsorption distance, bond lengths of CTE, and optimal designs of nano ring with appropriate adsorption energy. The charge transfer caused by CTE's adsorption onto Y9N9 is what causes the variations in DM of nano rings. Moreover the localization of the FMOs electron concentration confirms the types of interactions. The Y_9N_9 nano rings have potential use as a work-function and electron-based sensor for CTE. Furthermore, the projected recovery durations for CTE over Y_9N_9 are fairly long due to their strong interaction, and this means that CTE can be stored or eliminated from a

particular environment. Raman spectra provide additional evidence for the interaction between nanorings and CTE. RDG analysis indicated the presence of van der Waals (vdW) interactions in all cases and additionally revealed a strong attraction between CTE and the Al_9N_9 nanoring. The interaction between CTE and nano ring is stronger in aqueous medium compared to vacuum.

Declaration of competing interest

The authors declare that they have no known competing financial interests or personal relationships that could have appeared to influence the work reported in this paper.

Acknowledgment

Princess Nourah Bint Abdulrahman University Researchers Supporting Project number (PNURSP2025R13), Princess Nourah Bint Abdulrahman University., Riyadh, Saudi Arabia

Appendix A. Supplementary data

Supplementary data to this article can be found online at https://doi.org/10.1016/j.saa.2025.126148.

Data availability

Data will be made available on request.

References

[1] R. Wang, D. Zhang, W. Sun, Z. Han, C. Liu, A novel aluminium doped carbon nanotubes sensors for carbon monoxide, J. Mol. Struct. Theochem. 806 (2007) 93–97, https://doi.org/10.1016/j.theochem.2006.11.012.
[2] X. Ji, L. An, T. Chen, Adsorption of nitrogen oxides on Al-doped carbon nanotubes: the first principle study, Adsorption 26 (2020) 587–595, https://doi.org/10.1007/s10450-020-00218-3.
[3] Z. Lu, P. Lv, D. Ma, X. Yang, S. Li, Z. Yang, Detection of gas molecules on single Mn adatom adsorbed graphyne: a DFT-D study, J. Phys. D Appl. Phys. 51 (2018) 065109, https://doi.org/10.1088/1361-6463/aaa3b3.
[4] S. Kumar, M. Malhotra, H. Sharma, Adsorption of gas molecules on ultra thin pristine and doped graphene nanoribbons, Mater. Res. Express 5 (2018) 105007, https://doi.org/10.1088/2053-1591/aadaa8.
[5] S. Kumar, Meenakshi, H. Sharma, Effect of gas adsorption on graphene nanoribbons: a density functional theory, in: Mater. Today Proc., Elsevier Ltd, (2017) 10441-10445, doi: 10.1016/j.matpr.2017.06.396.
[6] E. Salih, A.I. Ayesh, Enhancing the sensing performance of zigzag graphene nanoribbon to detect NO, NO2 and NH3 gases, Sensors 20 (2020) 3932, https://doi.org/10.3390/2201443932.
[7] Y. Wang, N. Song, X. Song, T. Zhang, D. Yang, M. Li, A first principles study of gas adsorption on monolayer AlN sheet, Vacuum 147 (2018) 18–23, https://doi.org/10.1016/j.vacuum.2017.10.014.
[8] J. Beheshtian, Z. Bagheri, M. Kamfiroozi, A. Ahmadi, A theoretical study of CO adsorption on aluminium nitride nanotubes, Struct. Chem. 23 (2012) 653–657, https://doi.org/10.1007/s11224-011-9911-z.
[9] J. Beheshtian, A.A. Peyghan, Z. Bagheri, Selective function of Al12N12 nanocage towards NO and CO molecules, Comput. Mater. Sci 62 (2012) 71–74, https://doi.org/10.1016/j.commatsci.2012.05.041.
[10] A.A. Peyghan, H. Soleymanabadi, Z. Bagheri, First principles study of H2O and NH3 adsorption on the pristine and B-doped Al12N12 nanocluster, Iran, J. Sci. Technol. 39 (2015) 485–489. https://ijsts.shirazu.ac.ir.
[11] H.Y. Ammar, H.M. Badran, K.M. Eid, TM-doped B12N12 nanocage (TM=Mn,Fe) as sensor for CO, NO and NH3 gases: a DFT and TD-DFT study, Mater. Today Commun. 25 (2020) 101681, https://doi.org/10.1016/j.mtcomm.2020.101681.
[12] H. Huang, L. Liu, J. Wang, Y. Zhou, H. Hu, X. Ye, G. Liu, Z. Xu, H. Xu, W. Yang, Y. Wang, Y. Peng, P. Yang, J. Sun, P. Yan, X. Cao, B.Z. Tang, Aggregation caused quenching to aggregation induced emission transformation: a precise tuning based on BN-doped polycyclic aromatic hydrocarbons toward subcellular organelle specific imaging, Chem. Sci. 13 (2022) 3129–3139, https://doi.org/10.1039/D2SC00380E.
[13] D. Guo, H. Li, Z. Xu, Y. Nie, Development of pyrene-based MOFs probe for water content and investigations on their mechanochromism and acidochromism, J. Alloy. Compound. 968 (2023) 172004, https://doi.org/10.1016/j.jallcom.2023.172004.
[14] M. Kurban, I. Muz, Theoretical investigation of the adsorption behaviors of fluorouracil as an anticancer drug of pristine and B-, Al-, Ga-doped C36 nanotube, J. Mol. Liq. 309 (2020) 113209, https://doi.org/10.1016/j.molliq.2020.113209.
[15] I. Muz, M. Kurban, Zinc oxide nanoclusters and their potential application as CH4 and CO2 gas sensors: insight from DFT and TD-DFT, J. Comput. Chem. 43 (2022) 1839–1847, https://doi.org/10.1002/jcc.26986.
[16] S. Patel, P. Patel, D. Chodvadiya, N.N. Som, P.K. Jha, Adsorption performance of C12, B6N6 and Al6N6 nanoclusters towards hazardous gas molecules: a DFT investigation for gas sensing and removal application, J. Mol. Liq. 352 (2022) 118702, https://doi.org/10.1016/j.molliq.2022.118702.
[17] J.H. Li, J. Wu, Y.X. Wu, DFT exploration of sensor performances of two dimensional WO3 to ten small gases in terms of workfunction and band gap changes and I-V response, Appl. Surf. Sci. 546 (2021) 149104, https://doi.org/10.1016/j.apsusc.2021.149104.
[18] S.M. Majhi, A. Mirzaei, H.W. Kim, S.S. Kim, Reduced graphene oxide (Rgo)-loaded metal oxide nanofibre gas sensors: an overview, Sensors 21 (2021) 1–19, https://doi.org/10.3390/s21041352.
[19] X. Hou, Y. Ren, F. Fu, A density functional theory study on the electronic and adsorption characteristics of cyclo M9N9 (M=B and Al), J. Mol. Model. 26 (2020) 260, https://doi.org/10.1007/s00894-020-04520-3.
[20] H. Sajid, K. Ayub, T. Mahmood, Sensing behavior of monocyclic C18 and B9N9 analogues toward chemical warfare agents (CWAs): quantum chemical approach, Surface. Interfac. 30 (2022) 101912, https://doi.org/10.1016/j.surfin.2022.101912.
[21] X. Hou, X. Song, Y. Ren, W. Dong, Theoretical investigations of the interaction between B9N9 ring and nine adamantine derivatives, Comput. Theor. Chem. 1207 (2022) 113512, https://doi.org/10.1016/j.comptc.2021.113512.
[22] I. Muz, M. Kurban, A first principles evaluation on the interaction of 1,3,4-oxadiazole with pristine and B-, Al-, Ga-doped C60 fullerenes, J. Mol. Liq. 335 (2021) 116181, https://doi.org/10.1016/j.molliq.2021.116181.
[23] I. Muz, Enhanced adsorption of fluoroquinolone antibiotic on the surface of Mg-, Ca-, Fe-, and Zn-doped C60 fullerenes: DFT and TD-DFT approach, Mater. Today Commun. 31 (2022) 103798, https://doi.org/10.1016/j.mtcomm.2022.103798.
[24] M. Kurban, I. Muz, Size-dependent adsorption performance of ZnO nanoclusters for drug delivery applications, Struct. Chem. 34 (2023) 1061–1071, https://doi.org/10.1007/s11224-022-02063-2.
[25] I. Muz, F. Goktos, M. Kurbon, A density functional theory study on favipiravir drug interaction with BN-doped C60 heterofullerene, Physica E: Low Dimen. Syst. Nanostruct. 135 (2022) 114950, https://doi.org/10.1016/j.physe.2021.114950.
[26] C.E. Insmeirer, L. Wallman, L. Faxius, J. Schouenborg, L.M. Bjursten, N. Danielsen, Soft tissue reactions evoked by implanted gallium phosphide, Biomaterials 29 (2008) 4598–4604, https://doi.org/10.1016/j.biomaterials.2008.08.028.
[27] S.A. Jewett, M.S. Makowski, B. Andrews, M.J. Manfra, Gallium nitride is biocompatible and non-toxic before and after functionalization with peptides, Acta Biomater. 8 (2012) 728–733, https://doi.org/10.1016/j.actbio.2011.09.038.
[28] N. Wang, H. Wang, C. Tang, S. Lei, W. Shen, C. Wang, G. Wang, Z. Wang, L. Wang, Toxicity evaluation of boron nitride nanospheres and water soluble boron nitride in caenorhabditis elegans, Int. J. Nanomed. 12 (2017) 5941–5957, https://doi.org/10.2147/IJN.S130960.
[29] R. Duncan, R. Gaspar, Nanomedicine(s) under the microscope, Mol. Pharm. 8 (2011) 2101–2141, https://doi.org/10.1021/mp200394t.
[30] Y. Yin, J. Cervenka, N.V. Medhekar, Molecular dipole-driven electronic structure modification of DNA/RNA nucleobases on graphene, J. Phys. Chem. Lett. 8 (2017) 3087–3094, https://doi.org/10.1021/acs.jpclett.7b01283.
[31] S.S.N.A.S.I. Ishaat, M.K.M. Islam, M.R. Islam, Synthesis, spectroscopic characterization, antimicrobial activity, molecular docking and DFT studies of proton transfer (H-bonded) complex of 8-aminoquinoline (donor) with chloranilic acid (acceptor), J. Biomol. Struct. Dyn. 40 (2022) 12194–12208, https://doi.org/10.1080/07391102.2021.1969280.
[32] N. Elangovan, N. Arumugam, A.I. Almansour, S. Mathew, S. Djearamane, L. S. Wong, S. Kayarohanam, Synthesis, solvent role, absorption and emission studies of cytosine derivative, Heliyon 10 (2024) e28623, https://doi.org/10.1016/j.heliyon.2024.e28263.
[33] G.H. Shahnazari, M.D. Ganji, Understanding structural and molecular properties of complexes of nucleobases and Au13 golden nanocluster by DFT calculations and DFT-MD simulation, Sci. Rep. 11 (2021) 435, https://doi.org/10.1038/241598-020-80161-z.
[34] J. Xue, X. Guo, X. Wang, Y. Xiao, Density functional theory studies of cytosine analogues for inducing double-proton transfer with guanine, Sci. Rep. 10 (2020) 9671, https://doi.org/10.1038/s41598-020-66530-8.
[35] H. -K. Kim, D. H. Kim, Density functional theory calculations of the adsorption of cytosine on Si(100), Bull. Korean Chem. Soc. doi: 10.1002/bkcs.12108.
[36] M.T. Baei, M.R. TAghartapeh, E.T. Lemeski, A. Soltani, A computational study of adenine, uracil and cytosine adsorption upon AlN and BN nanocages, Phys. B Condens. Matter. 444 (2014) 6–13, https://doi.org/10.1016/j.physb:2014.03.013.
[37] H. Farooqui, A. Yadav, B.K. Pandey, Hydroxyl radical reactivity with cytosine and thymine: a computational study, J. Phys. 1849 (2021) 012029, https://doi.org/10.1088/1742-6596/1849/1/012029.
[38] H. Yang, H. Mei, F. Seela, Pyrrolo-dC metal-mediated base pairs in the reverse Watson-Crick double helix: enhanced stability of parallel DNA and impact of 6-pyridinyl residues on fluorescence and silver-ion binding, Chem. A Eur. J. 21 (2015) 10207–10219, https://doi.org/10.1002/chem.201500582.
[39] S. Ali, B. Lone, Density functional investigation of cytosine on platinum decorated graphene, AIP Conf. Proc. 2335 (2021) 080001, https://doi.org/10.1063/5.0043626.
[40] E.M. Mohammadi-Manesh, M. Mir-Mahdevar, Adsorption behavior of guanine, adenine, thymine, and cytosine nucleobases of DNA on zinc oxide-graphene nanosensor: A DFT study, Synth. Met. 267 (2020) 116486, https://doi.org/10.1016/j.synthmet.2020.116486.

[41] J. A. Jones, M. Mosca, Implementation of a quantum algorithm on a nuclear magnetic resonance quantum computer, 109 (1998) 1648-1653, doi: 10.1063/1.476739.
[42] S. Ali, B. Lone, Adsorption of cytosine on Si and Ge doped graphene: a DFT study, Mater. Today Proc. 80 (2023) 774–781, https://doi.org/10.1016/j.matpr.2022.11.085.
[43] T. Fan, Y. Cheng, Y. Wu, S. Liu, X. Tang, Y. He, S. Liao, X. Zheng, T. Zhang, Y. Qi, Y. Zhang, High performance TadA-8e derived cytosine and dual base editors with undetectable off-target effects in plants, Nature Commun. 15 (2024) 5103, https://doi.org/10.1038/s41467-024-49473-w.
[44] S.J. Parkinson, S.D.P. Fielden, M. Thomas, A.J. Miller, P.D. Topham, M.J. Derry, R. K. O'Reilly, Harnessing cytosine for tunable nanoparticle self assembly behavior using orthogonal stimuli, Macromolecules 25 (2024) 4905–4912, https://doi.org/10.1021/acs.biomac.4c00352.
[45] H. Li, X. Xu, Y. Liu, Y. Hoo, Z. Xu, Fluorophore molecule loaded in Tb-MOF for dual channel florescence chemosensor for consecutive visual detection of bacterial spores and dichromate anion, J. Alloy. Compound. 944 (2023) 169138, https://doi.org/10.1016/j.jallcom.2023.169138.
[46] S. Schlucker, Surface enhanced Raman spectroscopy, concepts and chemical applications, Angew. Chem. Int. Ed. 53 (2014) 4756–4795, https://doi.org/10.1002/anie.201205748.
[47] F. Goebel, A. Yakovlev, A.L. Pozniak, E. Vinogradova, G. Boogaerts, R. Hoetelmans, M.P.D. Bethune, M. Peeters, B. Woodfall, Short-term antiviral activity of TMC278-s novel NNRTI- in treatment-naive HIV-1-infected subjects, AIDS 20 (2006) 1721–1726, https://doi.org/10.1097/01.aids.000024818.65215.bd.
[48] Gaussian 16, Revision A.03, M. J. Frisch, G. W. Trucks, H. B. Schlegel, G. E. Scuseria, M. A. Robb, J. R. Cheeseman, G. Scalmani, V. Barone, G. A. Petersson, H. Nakatsuji, X. Li, M. Caricato, A. V. Marenich, J. Bloino, B. G. Janesko, R. Gomperts, B. Mennucci, H. P. Hratchian, J. V. Ortiz, A. F. Izmaylov, J. L. Sonnenberg, D. Williams-Young, F. Ding, F. Lipparini, F. Egidi, J. Goings, B. Peng, A. Petrone, T. Henderson, D. Ranasinghe, V. G. Zakrzewski, J. Gao, N. Rega, G. Zheng, W. Liang, M. Hada, M. Ehara, K. Toyota, R. Fukuda, J. Hasegawa, M. Ishida, T. Nakajima, Y. Honda, O. Kitao, H. Nakai, T. Vreven, K. Throssell, J. A. Montgomery, Jr., J. E. Peralta, F. Ogliaro, M. J. Bearpark, J. J. Heyd, E. N. Brothers, K. N. Kudin, V. N. Staroverov, T. A. Keith, R. Kobayashi, J. Normand, K. Raghavachari, A. P. Rendell, J. C. Burant, S. S. Iyengar, J. Tomasi, M. Cossi, J. M. Millam, M. Klene, C. Adamo, R. Cammi, J. W. Ochterski, R. L. Martin, K. Morokuma, O. Farkas, J. B. Foresman, and D. J. Fox, Gaussian, Inc., Wallingford CT, 2016.
[49] D. Rappoport, F. Furche, Property-optimized Gaussian basis set for molecular response calculations, J. Chem. Phys. 133 (2010) 134105, https://doi.org/10.1063/1.3484283.
[50] GaussView, Version 6.1, R. Dennington, T. A. Keith, J. M. Millam, Semichem Inc., Shawnee Mission, KS, 2016.
[51] N.M. O'Boyle, A.L. Tenderholt, K.M. Langner, Cclib: a library for package independent computational chemistry algorithms, J. Comput. Chem. 29 (2008) 839–845, https://doi.org/10.1002/jcc.20823.
[52] T. Lu, F. Chen, Multiwfn: a multifunctional wavefunction analyzer, J. Comput. Chem. 33 (2012) 580–592, https://doi.org/10.1002/jcc.22885.
[53] W. Humphrey, A. Dalke, K. Schulten, VMD: visual molecular dynamics, J. Mol. Graph. 14 (1996) 33–38, https://doi.org/10.1016/0263-7855(96)00018-5.
[54] N. Wazzan, P.K. Jha, Single atom catalysts supported on cyclo[18]carbon and its allotropes (B9N9 andAl9N9) for the hydrogen evolution and oxygen evolution reactions, Surface. Interfac. 42 (2023) 103319, https://doi.org/10.1016/j.surfin.2023.103319.
[55] L.S. Barbosa, E. Moreira, L. Villegas-Lelovsky, R. Paupitz, D.L. Azevdo, A DFT comparative study of cyclo[18] nanorings, BN and BCN, J. Clust. Sci. 34 (2023) 1465–1473, https://doi.org/10.1007/s10876-022-02313-7.
[56] F. Pichierri, Boron-nitrogen analogues of cyclo[18]carbon, Chem. Phys. Lett. 738 (2020) 136860, https://doi.org/10.1016/j.cplett.2019.136860.
[57] S.D. Dabhi, B. Roondhe, P.K. Jha, Nucleobases decorated boron nitride nanoribbon for electrochemical biosensing: a dispersion corrected DFT study, PCCP 20 (2018) 8943–8950, https://doi.org/10.1039/C7CP08145F.
[58] R. Sainda, D. Chodvadiya, P.K. Jha, A DFT study of Mg9O9 nanoring for gas sensing and removal applications, J. Mol. Liq. 397 (2024) 124121, https://doi.org/10.1016/j.molliq.2024.124121.
[59] J. Panchal, A. Gauswami, D. Chodvadiya, H. Jadeja, P.K. Jha, Adsorption performance of CO, NO and NH3 hazardous gas molecules over B9N9 and Al9N9 nanorings: acumen from density functional theory, Mater. Chem. Phys. 311 (2024) 128565, https://doi.org/10.1016/j.matchemphys.2023.127565.
[60] Z. Ullah, P.M. Sonawane, Y.S. Mary, Y.S. Mary, C.Y. Panicker, D.G. Churchill, A foundational theoretical $Al_{12}E_{12}$(E=N, P) adsorption and quinolone docking study: cage-quinolone pairs, optics and possible therapeutic and diagnostic applications, J. Biomol. Struct. Dyn. 41 (2023) 3630–3646, https://doi.org/10.1080/07391102.2022.2053742.
[61] J.S. Al-Otaibi, Y.S. Mary, Y.S. Mary, A. Mondal, N. Acharjee, D.S.R. Nair, Investigation of the interaction of thymine drugs with Be12O12 and Ca12O12 nanocages: A quantum chemical study, Spectrochim. Acta 308 (2024) 123728, https://doi.org/10.1016/j.saa.2023.123728.
[62] J.S. Al-Otaibi, Y.S. Mary, Y.S. Mary, G. Serdaroglu, Adsorption of adipic acid in Al/B-N/P nanocges: DFT investigations, J. Mol. Model. 27 (2021) 113, https://doi.org/10.1007/s00894-021-04742-z.
[63] D. Zhao, Y. Li, M. Xu, Z. Li, H. Zhang, L. Yu, Identification of sulfur gases (environmental pollution) by BeO fullerenes: a DFT study, J. Mol. Liq. 343 (2021) 117528, https://doi.org/10.1016/j.molliq.2021.117528.
[64] Z. Ullah, P.M. Sonawane, Y.S. Mary, Y.S. Mary, P. Mane, B. Chakraborty, D. G. Churchill, Theoretical model study of adsorbed antimalarial-graphene dimmers: doping effects, photophysical parameters, intermolecular interactions, edge adsorption, and SERS, J. Biomol. Struct. Dyn. 40 (2022) 13581–13592, https://doi.org/10.1080/07391102.2021.1990129.
[65] Z. Ullah, H.J. Kim, Y.S. Mary, H.W. Kwon, Insights into caffeine adsorption on the surface of corannulene: A sensor study, J. Mol. Liq. 368 (2022) 120592, https://doi.org/10.1016/j.molliq.2022.120592.
[66] G. Venkatesh, Y. Sixto-Lopez, P. Vennila, Y.S. Mary, J. Correa-Basurto, Y.S. Mary, A. Manikandan, An investigation on the molecular structure, interaction with metal clusters, anti-ovid-19 ability of 2-deoxy-D-glucose: DFT calculations, MD and docking simulations, J. Mol. Struct. 1258 (2022) 132678, https://doi.org/10.1016/j.molstruc.2022.132678.
[67] Z. Ullah, S. Subramanian, H. Lim, N.A. Dogan, J.S. Lee, T.S. Nguyen, C.Y. Yavuz, Highly selective and scalable molecular fluoride sensor for naked-eye detection, ACS Appl. Mater. Interfaces (2024), https://doi.org/10.1021/acsami.4c01187.
[68] J.S. Al-Otaibi, Y.S. Mary, Y.S. Mary, N. Acharjee, D.G. Churchill, Theoretical study of glycoluril by highly symmetrical magnesium oxide Mg12O12 nanostructure: adsorption, detection, SERS enhancement and electrical conductivity study, J. Mol. Model. 28 (2022) 332, https://doi.org/10.1007/s00894-05332-3.
[69] J.S. Al-Otaibi, Y.S. Mary, Y.S. Mary, Understanding the mechanism of thioguanine's binding to Ag6 and bimetallic (Ag3-Au3 andAg3-Cu3) clusters, J. Mol. Struct. 1265 (2022) 133415, https://doi.org/10.1016/j.molstruc.2022.133415.
[70] J.S. Al-Otaibi, Y.S. Mary, Y.S. Mary, Adsorption of a thione bioactive derivative over different silver/gold clusters – DFT investigations, Comp. Theor. Chem. 1207 (2022) 113497, https://doi.org/10.1016/j.comptc.2021.113497.
[71] J.S. Al-Otaibi, Y.S. Mary, Y.S. Mary, S. Kaya, G. Serdaaroglu, DFT computational study of trihalogenated aniline derivative's adsorption onto graphene/fullerene/fullerene-like nanocages, X12Y12 (X=Al, B and Y = N,P), J. Biomol. Struct. Dyn. 40 (2022) 8630–8643, https://doi.org/10.1080/07391102.2021.1914172.
[72] A.S. Kazachenko, N. Issaoui, A. Sagaama, Y.N. Malyar, O. Al-Dossary, L. G. Bousiakou, A.S. Kazachenko, A.V. Miroshnokova, Z, Xiang, Hydrogen bonds interactions in biuret-water clusters: FTIR, X-ray diffraction, AIM, DFT, RDG, ELF, NLO analysis, J. King Saud Univ. – Sci. 34 (2022) 102350, https://doi.org/10.1016/j.jksus.2022.102350.